


Synthesis and Characterization UV-Curable Waterborne Polyurethane Acrylate/ Al_2O_3 Nanocomposite Coatings Derived from *Jatropha* Oil Polyol

Suhaini Mamat^{1,2,*} , Luqman Chuah Abdullah^{1,3,*}, Min Min Aung^{3,5}, Suraya Abdul Rashid^{1,4}, Mek Zah Salleh⁶, Sariah Saalah⁷, Emiliana Rose Jusoh³, Marwah Rayung³

¹ Department of Chemical and Environmental Engineering, Faculty of Engineering, Universiti Putra Malaysia, Serdang 43400, Selangor, Malaysia; suhainim@micet.unikl.edu.my; chuah@upm.edu.my (L.C.A.);

² School of Environment and Polymer Engineering Technology, Malaysian Institute of Chemical and Bioengineering Technology (MICET), Universiti Kuala Lumpur, Taboh Naning, Alor Gajah 78000, Melaka, Malaysia

³ Higher Institution Centre of Excellence Wood and Tropical Fibre (HICoE), Institute of Tropical Forestry and Forest Products, Universiti Putra Malaysia, Serdang 43400, Selangor, Malaysia; minmin_aung@upm.edu.my (M.M.A.); tintahikmah@gmail.com (E.R.J.); marwahrayung@yahoo.com (M.R.);

⁴ Institute of Nanoscience and Nanotechnology, University Putra Malaysia, Serdang 43000, Selangor, Malaysia suraya_ar@upm.edu.my (S.A.R.);

⁵ Department of Chemistry, Faculty of Science and Technology, Universiti Putra Malaysia, Serdang 43400, Selangor, Malaysia

⁶ Radiation Processing Technology Division, Malaysian Nuclear Agency, Kajang 43000, Selangor, Malaysia; mekzah@nuclearmalaysia.gov.my (M.Z.S.);

⁷ Chemical Engineering Programme, Faculty of Engineering, Universiti Malaysia Sabah, Jalan UMS, Kota Kinabalu 88400, Sabah, Malaysia; s_sariah@ums.edu.my (S.S.);

* Correspondence: suhainim@unikl.edu.my (S.M.); chuah@upm.edu.my (L.C.A.);

Scopus Author ID 57193830517

Received: 28.01.2022; Accepted: 12.03.2022; Published: 3.04.2022

Abstract: A new UV-curable waterborne polyurethane acrylate/alumina (UV-WPUA/ Al_2O_3) coatings were successfully developed. The waterborne polyurethane acrylate (WPUA) dispersion was synthesized by reacting *jatropha* oil polyol (JOL) with isophorone diisocyanate (IPDI), 2,2-dimethylol propionic acid (DMPA), and 2-hydroxyethyl methacrylate (HEMA) via in-situ and anionic self-emulsifying methods. The WPUA/ Al_2O_3 dispersion was formulated by various sonicating concentrations of alumina nanoparticles (0.3, 0.6, 0.9, and 1.2 wt%) into WPUA dispersion. The UV-WPUA/ Al_2O_3 coatings were obtained with 75 wt% oligomers, 25 wt% monomer trimethylolpropane triacrylate (TMPTA), and 3 wt% of a commercial photoinitiator (benzophenone) for UV-curing were used. The effect of Al_2O_3 nanoparticles on WPUA coatings was analyzed by FTIR, surface morphology, and coating performance properties such as pendulum hardness, pencil hardness, scratch resistance, and adhesion test. FTIR revealed the formation of JOL, neat UV-WPUA, and UV-WPUA/ Al_2O_3 coatings, respectively. FESEM/EDX demonstrated that Al_2O_3 nanoparticles at the lower loading (up to 0.6 wt%) were well-dispersed correlated with contact angle (CA). The hardness property can reach 63.4% at the lower concentration of the Al_2O_3 addition 0.6 wt%. The adhesive strength, scratch hardness, and scratch resistance were greatly improved to 5B, 5H, and 2N, respectively. The preparation method offered in this study is an effective and convenient approach to producing UV-WPUA/ Al_2O_3 coatings. The enhancement of the properties with the lesser concentration of Al_2O_3 nanoparticles (≤ 0.6 wt%) addition in this study shows a new promising potential as surface coating application for several major industrial areas, such as marine, transportation, and biomedical field with major economic and environmental benefits.

Keywords: emulsion polymerization; scratch resistance; UV-curing; waterborne coating; nanocomposite coating; polyurethane acrylate; nanoalumina; bio-based coating.

© 2022 by the authors. This article is an open-access article distributed under the terms and conditions of the Creative Commons Attribution (CC BY) license (<https://creativecommons.org/licenses/by/4.0/>).

1. Introduction

Vegetable oils feedstock and WPUA based production are getting attention from researchers and academicians to utilize in biopolymer polyurethane composites coating due to their renewable, ecofriendly nature, sustainability, ease of processing, and economical [1]. Compared to mineral-based, the price of raw material, jatropha oil (JO) is low and will be further reduced if it becomes a commercial crop. The cost of converting JO to jatropha oil polyol (JOL) is also low. Furthermore, no or less organic solvent was used to produce the water-based system. The main organic solvents such as butanone, cyclohexanone, ethyl acetate, and toluene are commonly used in conventional coatings not only affect the environment, but some contain volatile isocyanate that will harm human health [2,3]. Growing concern over this issue has prompted the urethane coating industry to move toward a water-based system. Compared to their solvent counterparts, waterborne polyurethane (WPU) has an excellent film-forming capacity, low-temperature resistance, and is less expensive [4-6]. WPU can offer the advantages of being non-toxic, non-flammable, viscosity and flow properties independent of molecular weight, the absence of external emulsifiers, environmental safety, good adhesion, and rheology characteristics [7-11]. However, WPU still has weaknesses usually faced by a traditional polymer, which is a short lifetime resulting from physical damages such as scratches and microcracks, which will subsequently propagate to large cracks, leading to final fracture [12].

JO has an excellent potential to be used as the raw material for polyurethane (PU) bio-coating due to its high unsaturated fatty acid content. Currently, JOL derived from jatropha oil appears to be a promising candidate as a feedstock for polyurethane adhesives [13-16], coatings [17-23], and polymer electrolytes [24-26]. A great deal of effort has been devoted to developing biobased polyurethane coatings structure, morphology, and properties by introducing new chemical structures in the backbone chain so that the performance of biobased polyurethane coatings produced comparable to mineral-based polyurethane.

The UV-curable polymer, polyurethane acrylate (PUA), a segmented PU resin with acrylic functionality, is a good candidate for numerous coating applications [27]. WPUA is a modified polyurethane, concurrently owning the advantages of polyurethane and polyacrylate, known as the third generation of WPU [28]. WPUA emulsion has the advantages of small particle size, narrow distribution, good stability, good film performance, and solid content of 45 wt.% [29]. UV-curable waterborne technology is a merging method that could combine advantages and overcome drawbacks of waterborne and UV-curable systems [30-32]. Several advantages offered by UV-curing such as very rapid cure at room temperature, versatile formulation range, VOC complaint, reduction in required floor space, lower energy consumption, high automated production, ability to coat heat-sensitive substrates, minimal waste, long shelf-life, immediate handling of coated product, and low capital required for curing equipment [33-36]. Compared to conventional thermal-curable coatings, UV-curable coating always shows better comprehensive performance, such as excellent film-forming property and high thermal stability. Other researchers have also acknowledged UV-curing technology as 5E, which stands for Efficiency, Energy saving, and economical and

environmentally friendly [37-43]. Furthermore, conventional drying of WPU takes a few days to cure [44], while WPU derived from JO requires 8 days at room temperature to be cured [45], and UV-curable coatings can be cured within seconds at room temperature [46]. Thus, a high drying rate is an additional benefit of UV curing.

The addition of inorganic or organic solid particles to polymers is a very common method used to improve their mechanical properties. For inorganic nanofiller, generally, the types of ceramic particles are SiO₂, Al₂O₃, ZnO, TiO₂, and CaCO₃. Compared to metallic or organic oxides, ceramic coatings provide a better coating due to their higher hardness and strength, even with a lower thickness [47-48]. SiO₂ is the most used and studied particle [49-54]. However, the weakness of silica-based fillers is that high loadings of the particles are generally required to show a significant enhancement in the scratch/abrasion resistance of the coating, and these high amounts can lead to various other formulation problems associated with viscosity, thixotropy, and film formation [55-56]. Al₂O₃ is an engineering ceramic material [57-58] with numerous interesting properties such as wear-resistance [59-61], good dielectric [62,63] application, resistance to acid and alkali at elevated temperature, excellent thermal conductivity, and can be obtained in high purity up to 99.5% [63-66]. Several studies reported on the incorporation of Al₂O₃ into 2K polyurethane coatings to enhance the scratch behavior of the coating. They concluded that the addition of hard particles did not reduce scratch damage as assessed by scratch width measurement [67,68]. For polyacrylic coating, one study cited that its scratch resistance is improved by adding Al₂O₃ nanoparticles [68]. Another study reported that inorganic filler, Al₂O₃ is a thermodynamically stable material with trigonal symmetry [69]. Due to its favorable physical properties, Al₂O₃ has been commonly used in the fabrication of high-performance nanocomposites [69,70]. Other authors [71] in their studies cited [72-76] that Al₂O₃ is one such ceramic particle that presents itself as an excellent choice of a nanofiller, owing to its extremely high hardness retention at elevated temperatures, bio-inertness, ability to enhance the pristine polymer's load-bearing ability, and exceptional corrosion resistance. Few studies on the effect of Al₂O₃ on petroleum-based polyurethane acrylate nanocomposite coatings for scratch and mar resistance and corrosion protection have been conducted. However, a systematic study of the effect of Al₂O₃ nanoparticles on the physical properties, mechanical properties, and other performances of polyurethane coatings has not been well demonstrated.

The goal of this study is to develop biobased and economic UV-WPUA/Al₂O₃ nanocomposite coatings, which have not been reported up to date. UV-curable WPUA/Al₂O₃ nanocomposite coatings have been considered a novel formation in the research on waterborne polyurethane nanocomposite coatings based on vegetable oil-based polyols generally jatropha oil-based polyols particularly. Al₂O₃ was used as a nanofiller at different weight percentages (0.3 wt% to 1.2 wt%) loading to study the variation in physical properties and mechanical performances and compared with the neat WPUA coating.

2. Materials and Methods

2.1. Materials.

The raw material and chemicals used in this study are listed in Table 1. JOL was produced by synthesizing non-edible grade jatropha oils, and all chemicals were reagent grade and used as received. The individual particle size Al₂O₃ was 20 nm, which is consistent with the vendor's specification on the suspension and a specific surface area of > 138 m²/g. It is

hydrophilic, nearly spherical, was supplied in white powder form, and 99 wt% purely γ - Al_2O_3 . Al_2O_3 nanoparticles used were of reagent grade/higher purity. A photoinitiator, bphenol, was selected and added to the formulation to generate free radical, which initiates polymer chain growth of the acrylate group to produce a thermosetting polymer.

Table 1. Materials for UV-WPUA/ Al_2O_3 coatings.

Designation	Chemical identification	Supplier
JO	Jatropha oil	BATC Development Berhad, Malaysia
H_2O_2	Hydrogen peroxide 30%	Merck, Germany
CH_3OH	Methanol	Merck, Germany
DMPA	2,2-bis(hydroxymethyl)propionic acid	Aldrich Chemicals
NMP	n-methyl pyrrolidone 98%	Aldrich Chemicals
IPDI	Isophrene diisocyanate	Aldrich Chemicals
HEMA	2-hydroxyethyl methacrylate	Aldrich Chemicals
DBTDL	Phthalic anhydride and dibutyltin dilaurate	Aldrich Chemicals
MEK	Ethyl methyl ketone	Meck, Germany
TEA	Triethylamine, 99%	System
FA	Formic acid	System
MgSO_4	Magnesium sulphate anhydrous	System
	Pyridine	System
Al_2O_3	Alumina nanoparticle, gamma, 99%, 20nm, Hydrophilic, specific surface area > 138 m^2/g , morphology: nearly spherical	Research nanomaterial, Inc, Houston, USA.
Bphenol	Benzophenol 50wt%	Ciba Specialty Chemicals Inc., Switzerland.
TMPTA	Trimethylolpropane triacrylate	Ciba Specialty Chemicals Inc., Switzerland.

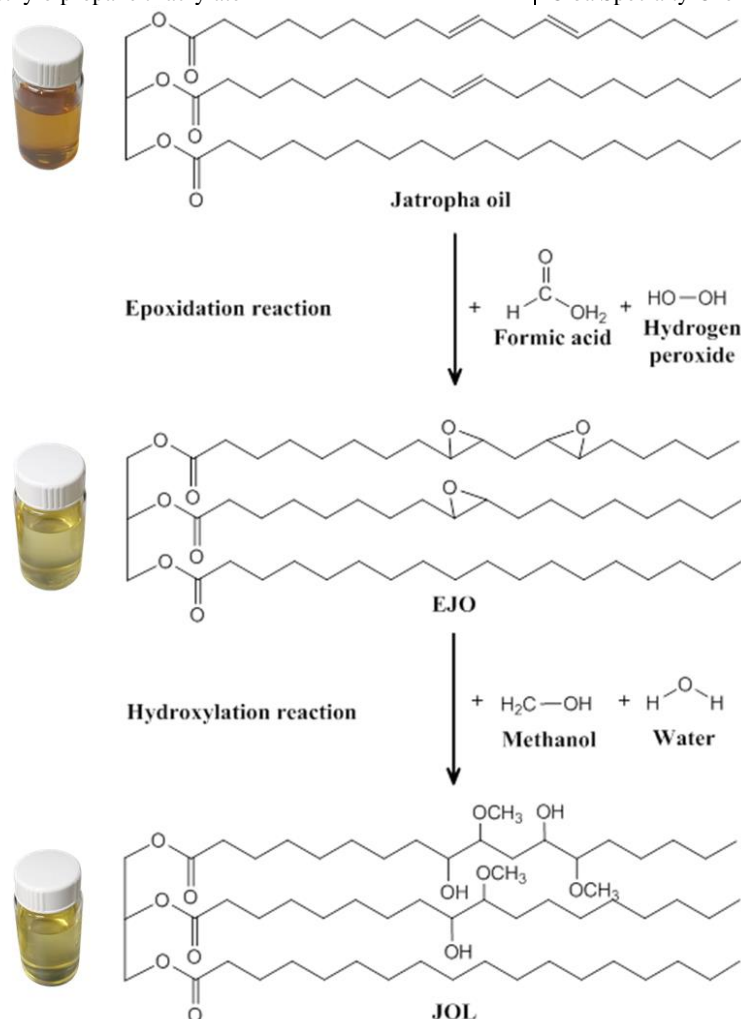


Figure 1. Synthesis route for epoxidized JO and polyol-based JO [3].

2.2. Synthesis of WPUA dispersion.

Briefly, epoxidized jatropha oils (EJO) were synthesized by the epoxidation method before being characterized by OOC value and FTIR analysis and further used for JOL synthesis. The JOL was produced by the hydroxylation method, and it was used for characterized hydroxyl value, FTIR analysis and further used for WPUA synthesis. Details of the synthesis route of JOL have been reported in the previous study by the same authors [5] with slight modifications. Figure 1 shows the elementary steps for the synthesis of the JOL.

Table 2. Sample designation and composition of WPUA/alumina dispersion.

Sample designation	Composition (Molar ratio)					(% Alumina)	Molecular Weight (g/mol)	Molecular weight distribution
	JOL (OH)	DMPA (OH)	IPDI (NCO)	HEMA (OH)	TEA			
A ₀ WPUA	0.1930	0.0729	0.2742	0.0768	0.0438	0.0	121783	1.092107
0.3A ₂₀ WPUA	0.1930	0.0729	0.2742	0.0768	0.0438	0.3	121871	1.095420
0.6A ₂₀ WPUA	0.1930	0.0729	0.2742	0.0768	0.0438	0.6	121958	1.111964
0.9A ₂₀ WPUA	0.1930	0.0729	0.2742	0.0768	0.0438	0.9	122113	1.135555
1.2A ₂₀ WPUA	0.1930	0.0729	0.2742	0.0768	0.0438	1.2	122359	1.146747

The preparation approach for WPUA oligomer is illustrated in Figure 2, and the formulation of the synthesis WPUA is shown in Table 2. 60 g JOL was added into a four-necked flask equipped with a reflux condenser, mechanical stirrer, dropping funnel, and the flask was placed in a silicone bath.

The system was performed under a dry N₂ atmosphere, continuously stirred until the temperature reached 60°C. Then, IPDI was slowly dropped wisely for 30 minutes under a constant temperature of 60°C. Afterward, a calculated amount of DBTDL was added, and the reaction mixture was heated to 80°C and kept at a temperature for 2 h to prepare the -NCO terminated prepolymer. Next, the mixture was reacted with a certain calculated amount of DMPA dissolved in a small amount of NMP at 80°C for another 2 h to attain the -NCO terminated prepolymer containing carboxy group. Then, the mixture was cooled to 60°C, and MEK was added to control the viscosity of the prepolymer. HEMA was dropped slowly and allowed to be reacted for another 3 h at 60°C to cap the entire terminal -NCO group. Then, polyurethane acrylate (PUA) oligomer was obtained, being cooled to 40°C, and the carboxylic acid group was neutralized by TEA for 30 minutes. A calculated amount of distilled water was dispersed into the system under vigorous stirring for 30 minutes. Finally, MEK was removed by vacuum distillation under low pressure, and WPUA oligomer was obtained.

2.3. Preparation of UV-WPUA/Al₂O₃ coatings.

The formulation of UV-curable WPUA/Al₂O₃ nanocomposite is indicated in Table 3. Al₂O₃ nanoparticles in the size range of 20 nm with loading composition of 0.3, 0.6, 0.9, and 1.2 wt% were dispersed in neat WPUA emulsion and sonicated for 35 minutes to minimize aggregated alumina particles. A series of nanocomposite coatings were obtained and coded as 0.3A₂₀WPUA, 0.6A₂₀WPUA, 0.9A₂₀WPUA and 1.2A₂₀WPUA, respectively.

TMPTA monomer and bphenol were added to different amounts of WPUA/Al₂O₃ dispersion; the mixture was homogenized at room temperature for 15 min with a homogenizer. The monomer and photoinitiator concentration were kept constant in all formulations. Thereafter, the formulated coatings were coated on a glass substrate (10 cm × 10 cm × 0.3 cm) using 120 bar coaters at 120 μm wet films thickness and given a flash off for an hour before being cured by a UV-curing machine with a high-pressure mercury lamp. The exposure time

was 10 s to get a completely dried coating. The film was considered fully cured after five passes under UV light based on a non-tackiness test using a finger (ASTM D1640). The coated substrate and film cured nanocomposite coatings were kept for further characterization.

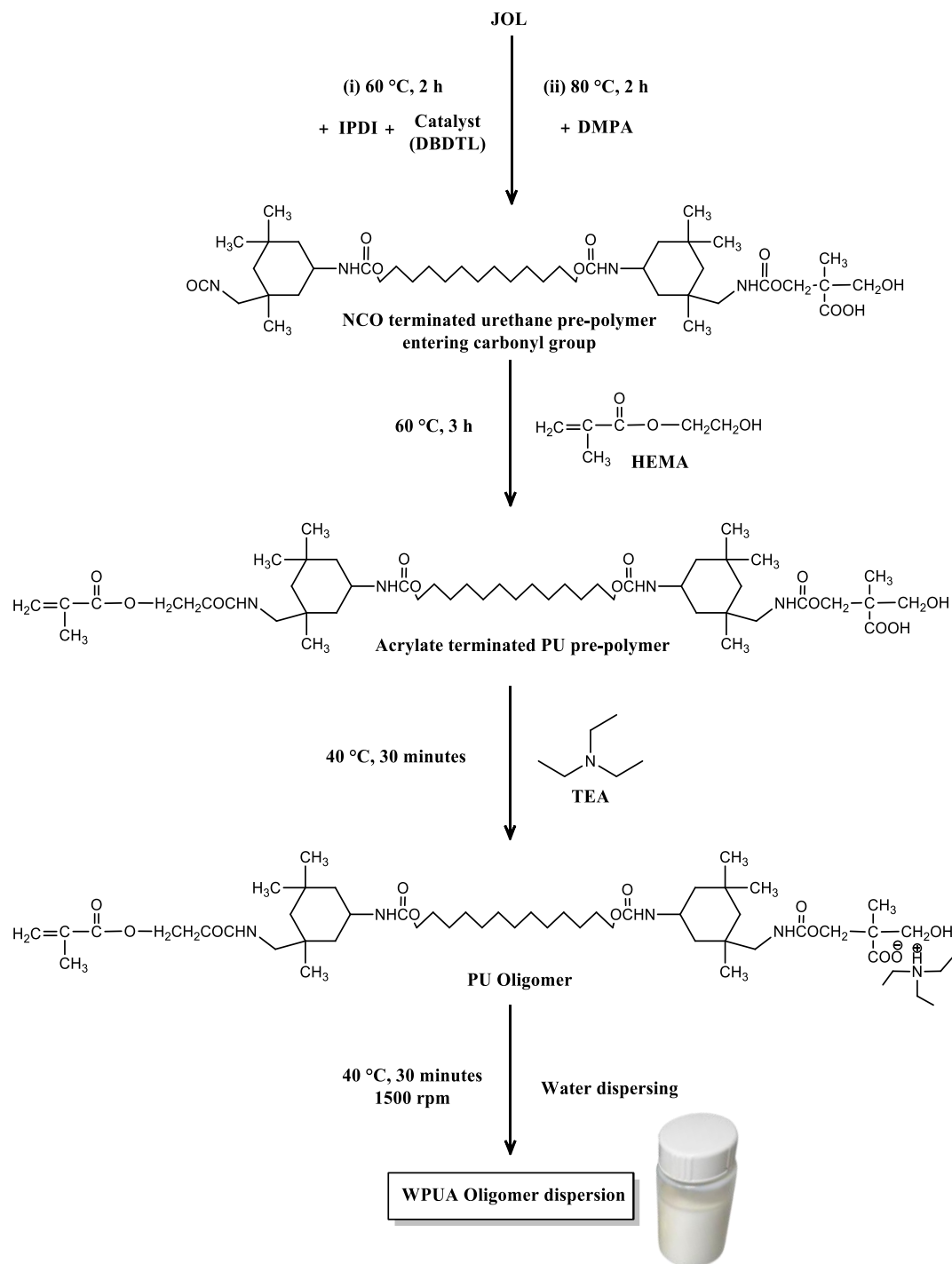


Figure 2. Synthesis route for WPUA dispersion.

Table 3. The formulation of UV-WPUAD/Al₂O₃ coatings.

Sample Code	Composition of materials (wt%)				
	Al ₂ O ₃	WPUA	TPMTA	Bphenol	Co- I
Neat WPUA	0.0	75.0	25	3	1
0.3A ₂₀ WPUA	0.3	74.7	25	3	1
0.6A ₂₀ WPUA	0.6	74.4	25	3	1
0.9A ₂₀ WPUA	0.9	74.1	25	3	1
1.2A ₂₀ WPUA	1.2	73.8	25	3	1

*Co-I: Co-initiator

The illustration of UV-WPUA/Al₂O₃ nanocomposite coating is schematically presented in Figure 3.

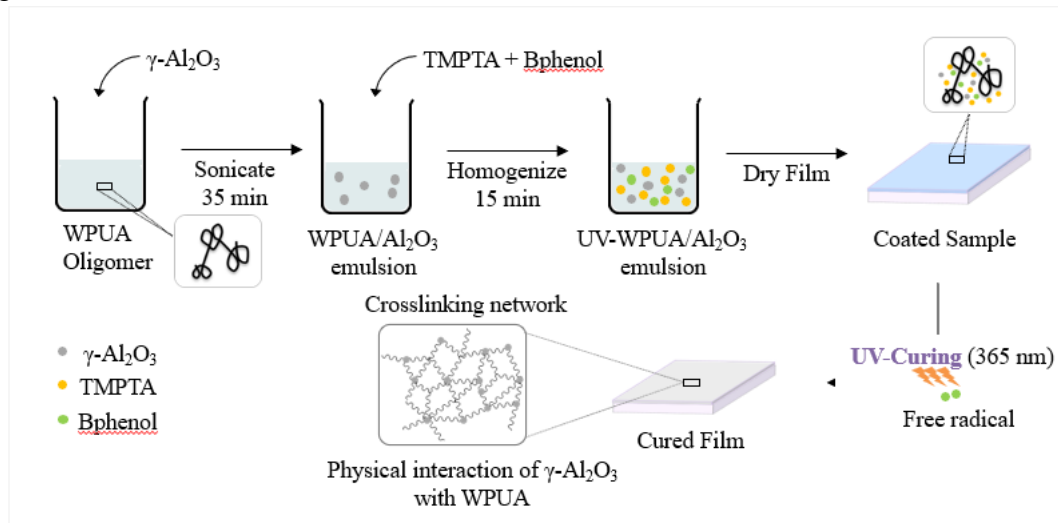


Figure 3. Schematic illustration of UV-WPUA/Al₂O₃ nanocomposite coating.

2.4. Characterization.

2.4.1. Physiochemical properties.

The presence of oxirane oxygen content, OOC (%) of EJO and acid value, and OH value of JOL was determined by the volumetric titration method according to AOCS Tentative Method Cd 9-57, revised 1963, ASTM D4662-03 Test and ASTM D4274-16, respectively [5]. OOC was conducted to check the disappearance of the oxirane ring during the synthesis of EJO process. Under the prescribed conditions of AOCS Cd 9-57 method, oxygen was titrated directly using a hydrobromic acid solution in glacial acetic acid. From the OOC measurement, the relative conversion to oxirane (RCO) value was calculated by the following Eq (1):

$$RCO = \frac{OOC_{exp}}{OOC_{theory}} \times 100\% \quad (1)$$

Where OOC_{exp} is the experimentally determined oxirane oxygen, and OOC_{theory} is the theoretical maximum oxirane oxygen. These parameters were calculated according to Eqs (2) and (3).

$$OOC_{exp} = \frac{1.60VN}{W_t} \times 100 \quad (2)$$

where V and N are the volume and normality of the HBr solution and W_t is the weight of the sample.

$$OOC_{theory} = \frac{IV_0/2A_i}{100+(IV_0/2A_i)A_0} \times 100 \quad (3)$$

where A_i (126.9) and A_o (16.0) are atomic masses of the iodine and oxygen, respectively, and IV_0 is the initial iodine value of the sample.

2.4.2. FTIR analysis.

IR analysis was performed in the wavenumber region of 4000 to 400 cm⁻¹ using an FTIR spectrometer (Bruker Tensor 11, Ettlingen, Germany) equipped with an attenuated total reflectance (ATR), which consists of a diamond disc as an internal reflection element. The spectrum of air was used as a background before each sample analysis. Background and sample spectra were taken in a room with a temperature around 21-23°C at a spectral resolution of 4 cm⁻¹, and for each measurement, 32 scans were performed. ATR-FTIR was used to confirm

the synthesis of EJO and JOL and demonstrate UV-WPUA formulations' photopolymerization following the conversion of acrylate double bonds on coating films after UV exposure.

2.4.3. Morphology studies.

UV-WPUA and UV-WPUA/Al₂O₃ coated morphologies of resulting nanocomposites were observed by Field emission scanning electron microscopy (FESEM, GeminiSEM*500 developed using Gemini technology by Carl Zeiss, Germany) equipped with a system for energy dispersive X-Ray spectrometer (EDX) to confirm the present of Al₂O₃ nanoparticles in the polymer matrix. EDX spectra were measured with the energy of the primary electron beam of 20 keV. Samples were coated with platinum (Quorum Q150T, sputter-coater, Kent, UK) in order to prevent sample charging.

2.5. Coating characterization.

2.5.1. Glossiness.

The influence of Al₂O₃ nanoparticles on the optical UV-WPUA coatings was measured in terms of 60° and 20° gloss according to ASTM Method D1033-61 (1977) by means of a gloss meter (Mirco-TRI-gloss, BYK-Gardner, Columbia, MD, USA). The measured gloss is an average standard of 10 measurements at angles incident light of 20°.

2.5.2. Contact angle.

The surface properties and wettability of neat UV-WPUA and UV-WPUA/Al₂O₃ coated films were measured by static contact angle (CA) measurement using the optical tensiometer instrument (Theta Lite, Biolin Scientific, Finland) equipped with a camera following the sessile liquid droplet method in the air at room temperature with 2 µL droplets of deionized water.

2.5.3. Pendulum hardness.

The hardness of UV-WPUA\Al₂O₃ coatings was determined by measuring the deflection angles of a pendulum oscillating on the coating samples according to the standard ASTM D4366 (Pendulum hardness tester, BYK-Gardner). The hardness value corresponded to the damping time of the pendulum from 6 to 3 (König pendulum). Hardness determination characterizes or forecasts the behavior of a coating subjected to such practical conditions as complying with the hardness definition.

2.5.4. Pencil hardness test.

The pencil hardness test is the Wolf-Wilburn method was used to measure the hardness or the qualitative determination of anti-scratch resistance of coatings according to the ASTM D-3363-05 [77]. The pencil test selection to measure anti-scratch resistance is due to its simplicity and acceptance in the field of surface characterization of industrial coating [78]. The test consists of using a set of pencils (Derwent Graphics, Workington, UK) with different hardness in a decreasing order to determine the first pencil that does not produce any mark on the coating surface. The hardness value in the Wolf-Wilburn scale, H_w (6B to 6H range of pencils), was used for the test. Then, the hardness of such a pencil is taken as the hardness of the coating.

2.5.5. Scratch test.

The scratch (macro) on the coated substrates was measured with the help of a mechanical scratch tester (Model: 413, Erichsen Scratch hardness Tester) in accordance with ASTM G 171. The scratching steel ball tip with a diameter of 1 mm was drawn in a circular motion on the coating substrates using a weight load varying from 0.1N to 10 N. The load that managed to penetrate or crack the films was recorded as the maximum scratch resistance of the coatings.

2.5.6. Adhesion test.

The cross-hatch adhesion test (Biuged, Guangzhou, China) follows ASTM D3359-02 and provides a qualitative evaluation of surface coating adhesion performance while dry through a visual examination. The kit consists of cross-hatch adhesion testers, a cutter blade, standard adhesive tape, magnifying glass, and a soft brush. A cross-hatch pattern was made by a cross-cut cutter on the surface of the coating, and the detached flakes of coatings were cleaned with a soft brush. Standard adhesive tape was applied over the cross-hatch cut, and the tape was pulled up quickly back upon itself as close to an angle of 180° as possible. The remaining coating was judged by comparison with descriptive illustrations in ASTM standard. The classification of the test result is shown in Table 4. The test was performed on three replicates of each coating system.

Table 4. The standard evaluation criteria for coating adhesion
Qualified Adhesion Requirement: Adhesion ≥ 4B

5B	The edges of the cuts are perfectly smooth, and there is no fall-off at the squares or the lattice.
4B	Small flakes of the coating fall off at the edge or intersections of the squares, and the total area of fall-off is less than 5%.
3B	Small flakes of coating fall off along the edges and at intersections of the squares, and the area of fall-off is between 5% and 15%.
2B	Flakes of coating fall off along the edges and at parts of the squares, and the area of fall-off is between 15% and 35%.
1B	Flakes of coating fall off along the edges of cuts in large ribbons and entire squares, and the area of fall-off is between 35% to 65%.
0B	Flaking and detachment is the access of 65%.

3. Results and Discussion

The synthesis mechanism of WPUA derived from JOL by *in situ* polymerization method, as illustrated in Figure 1 and Figure 2, involves three major steps. Firstly, JO was converted into EJO via epoxidation reaction process, followed by the second step, which is EJO was transformed into JOL via hydroxylation reaction process. In the third step, WPUA synthesis was prepared according to the conventional batch-feed process, in-situ polymerization method because this technique is most suitable, safe, and economical for small scale. EJO derived from JO was prepared with some modifications according to reported procedures in the literature [5,79,80].

Table 5. Physiochemical properties of JO, EJO, Polyol based-JO and WPUA dispersions.

Sample	Acid Value (mg of KOH/g)	OOC* (%)	Hydroxyl Number (mg of KOH/g)	Physical Appearance
JO	-	-	-	Liquid, Golden yellow
EJO	23.78±0.3	4.34±0.6	-	Liquid, Light Yellow
JOL	26.47±0.6	-	171±5.3	Liquid, Yellowish
WPUA	6.97±0.03	-	-	Emulsion, Milky white, no odor

*OOC = Oxirene oxygen content

3.1. Physicochemical properties.

Table 5 shows some of the physicochemical properties of EJO, JOL, and WPUA. The EJO and JOL samples are in liquid, while WPUA is in an emulsion form. The acid values of EJO and JOL are 23.78 and 26.47 mg of KOH/g, respectively. The higher acid value of EJO and JOL indicates that it contains a higher amount of free acid. The authors [81] reported that the resins with higher acid values contributed to an increase in the pendulum hardness rate of the coating. OOC values of EJO are about 4.34% indicating the percentage of epoxy groups present in the acid backbone, while the OH value of JOL is 171 mg of KOH/g. A pure color of the raw material, JO is golden yellow, and after the epoxidation and hydroxylation reaction, EJO and JOL are slightly brighter with light yellowish and yellowish colors, respectively. The color of WPUA dispersion is milky white. All these chemical characterizations are within the range of data that has already been performed by many researchers [5,82,83].

3.2. Chemical analysis.

The synthesized neat UV-WPUA and UV-WPUA/Al₂O₃ coatings were characterized by FTIR. Figure 4 and Figure 5 show the infrared spectra of JO, EJO, Polyols, neat WPUA, and WPUA/nano-Al₂O₃ composite coatings, respectively. Typically, the carbon-carbon double bonds are present in most vegetable oils, as shown in the characteristic peak of JO. The spectrum of JO in Figure 4(a) indicated a CH stretching of saturated fatty acid backbone at 2950 cm⁻¹ and 2858 cm⁻¹, which correspond to a stretching band of the terminal methyl group (CH₃) and methylene proton (CH₂) of triglyceride molecule, respectively. The peak around 1744 cm⁻¹ is attributed to the carbonyl group (C=O) of the triglyceride backbone. A significant functional group of unsaturated fatty acid was shown at 3009 cm⁻¹, which indicated the vinyl proton of unsaturation double bond (CH=CH). The double bond is quite strong in the JO, but it disappeared in the EJO in Figure 4(b) due to the consumption of double bonds in the epoxidation reaction to form epoxy rings.

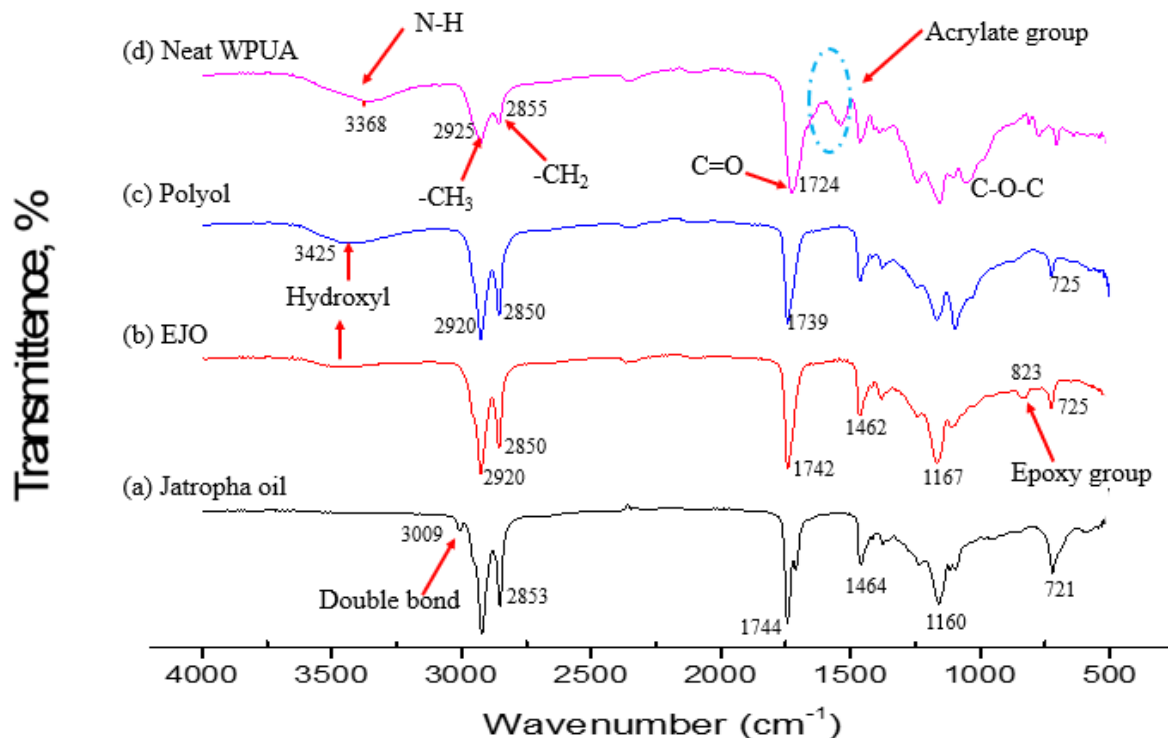


Figure 4. FTIR spectra of (a) JO; (b) EJO; (c) Polyols; (d) neat UV-WPUA coatings.

The broad absorbance of polyol at 3425 cm^{-1} in Figure 4(c) shifted to 3365 cm^{-1} in Figure 4(d), showing that the OH group was transformed into a hydrogen-bonded NH group. It is observed that isocyanate and hydroxyl groups in Figure 4(d) were not present in the spectrum, indicating that all monomers had completely reacted during polymerization/curing. Once polyol-based JO reacts with IPDI and HEMA to form PUA, the NCO group of IPDI responds with both hydroxyl polyol and HEMA to form a urethane bond (NHCOO). Figure (d) shows the absence of NCO band at 2270 cm^{-1} , and the presence of the N-H band at 3365 cm^{-1} reveals the occurrence of the polymerization process. The absorption peak of terminal methylene groups ($=\text{CH}_2$) observed at 1666 cm^{-1} indicates incorporating the C=O bond of HEMA into the polyurethane chains. Meanwhile, the stretching vibration is shown at $2859 - 2924\text{ cm}^{-1}$ and 1087 cm^{-1} correspond to methanediyl groups ($-\text{CH}_2-$), methyl groups ($-\text{CH}_3-$), and ether groups ($-\text{C}-\text{O}-\text{C}-$) respectively [84-86]. These findings have shown the successful synthesis of WPUA.

Figure 5 presented the comparison of the FTIR spectra WPUA according to the neat UV-WPUA coating and UV-WPUA/ Al_2O_3 coating with different compositions. The typical IR spectrum of the neat WPU showed bands near 3330 cm^{-1} (N-H stretching), 1700 cm^{-1} (C=O stretching), and 1540 cm^{-1} (C-N-H bending). The characteristic carbonyl group peak appearing at 1700 cm^{-1} region notify about the change in intermolecular bonding such as hydrogen bonding and dipole-dipole between carbonyl group. From the spectrum, UV-WPUA/ Al_2O_3 coatings did not reveal any -OH stretch as in spectra of Al_2O_3 , suggesting that the Al_2O_3 nanoparticles have been embedded into the WPUA matrices. Furthermore, all the spectra do not show significant changes in absorption peaks with the increase of Al_2O_3 nanoparticles composition, indicating that the incorporation of Al_2O_3 nanoparticles did not interfere with the curing process WPUA.

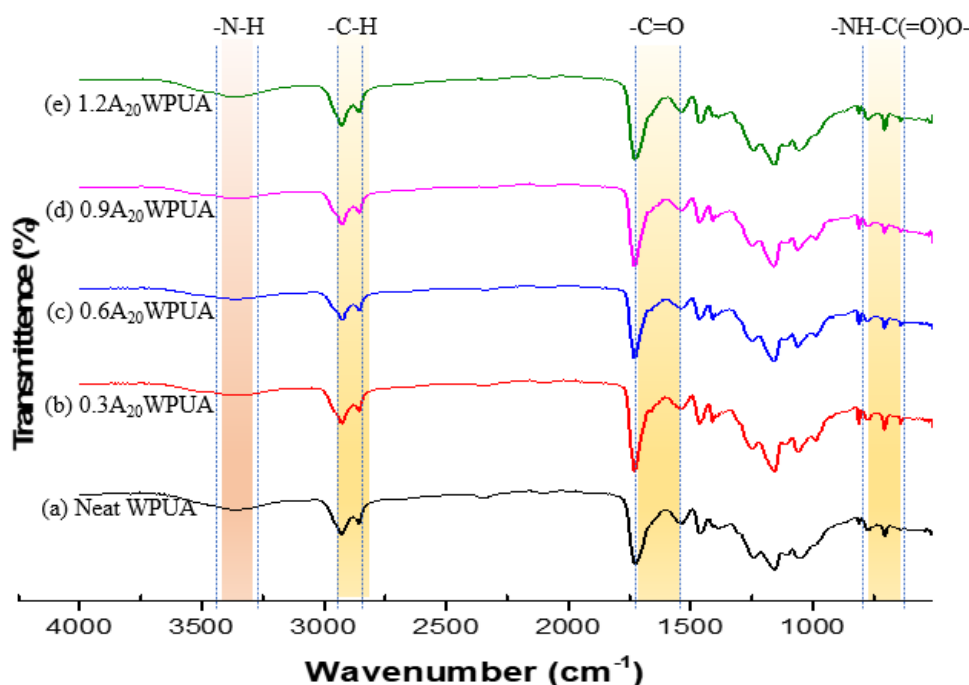
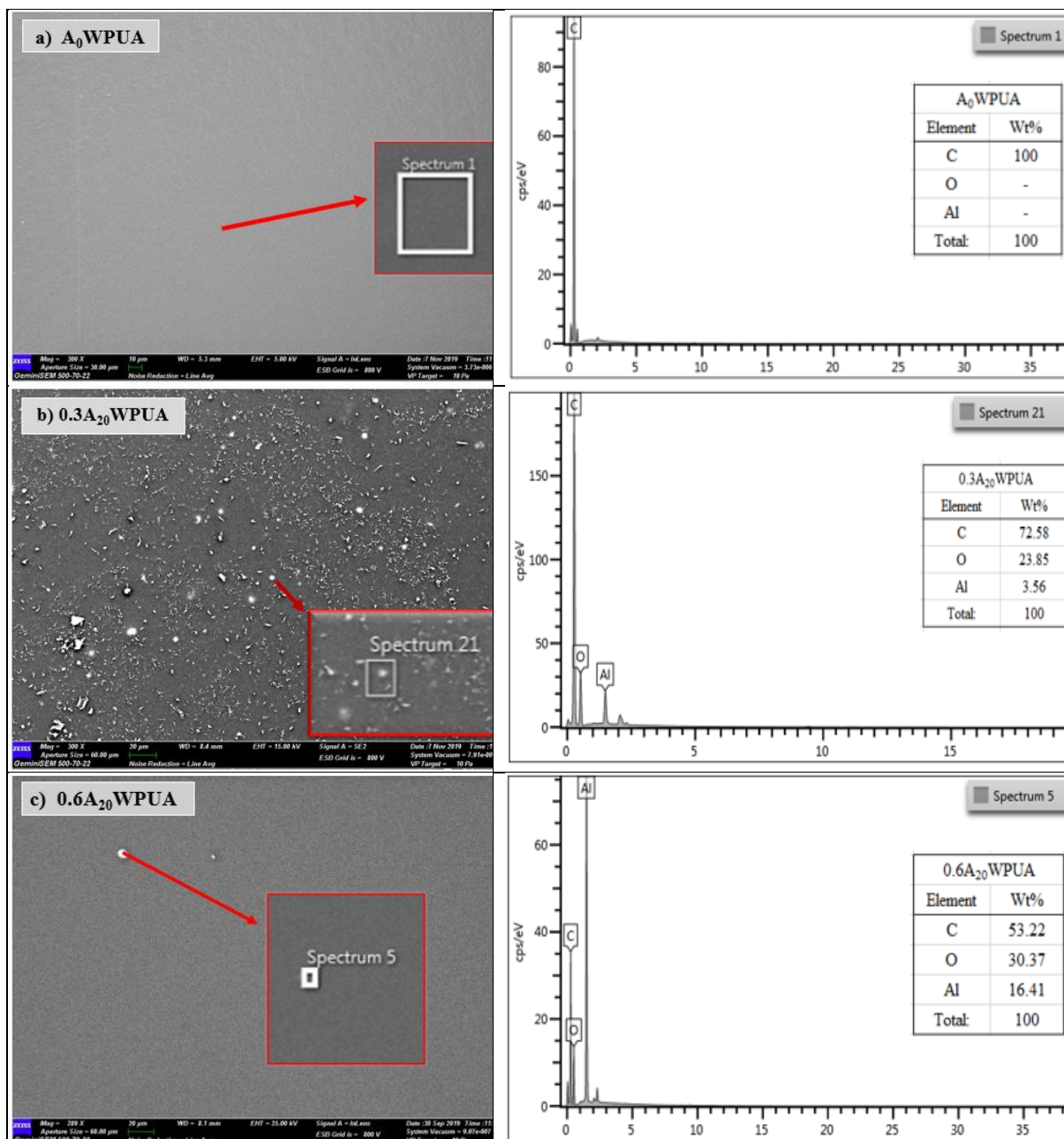


Figure 5. FTIR spectra for UV-cured WPUA filled various loading nano- Al_2O_3 coatings.

3.3. Microstructure.

In order to confirm the dispersibility of the Al_2O_3 nanoparticles to the WPUA dispersion, FESEM/EDX analysis was conducted, and the results are shown in Figure 6. Figure

6 shows the scanning electron micrographs of the synthesized WPUAs (neat WPUA coating and WPUA/Al₂O₃ nanocomposite coatings) at ×300000 magnifications with an acceleration voltage of 5 kV. FESEM images of neat UV-WPUA and UV-WPUA/Al₂O₃ coatings have clearly revealed the presence of one phase, and all the surface coatings were smooth uniform, and no cracks were detected. It means that the nanocomposite coatings show a better mixing of the soft and hard segments. The distribution of Al₂O₃ nanoparticles within the WPUA matrix was generally uniform, with no evidence of extensive settling. The images' bright dots and tread-like structures are attributed to the Al₂O₃ nanoparticles. The dispersion of Al₂O₃ nanoparticles in the WPUA matrix at lower loading (0.6 wt%), as shown in Figure 6(c), is found to be homogeneously dispersed throughout the WPUA matrix without any agglomeration. But agglomeration is seen at higher (0.9 and 1.2 wt%) loadings depicted in Figure 6(d) and Figure 6(e), respectively. In 0.6 wt% Al₂O₃ nanoparticles loading micrographs, well-dispersed nanoparticles throughout the entire surface could be attributed to the induced Van der Waals force between polymer and Al₂O₃ nanoparticles which exceeds the existing interparticle forces during sonication [87].



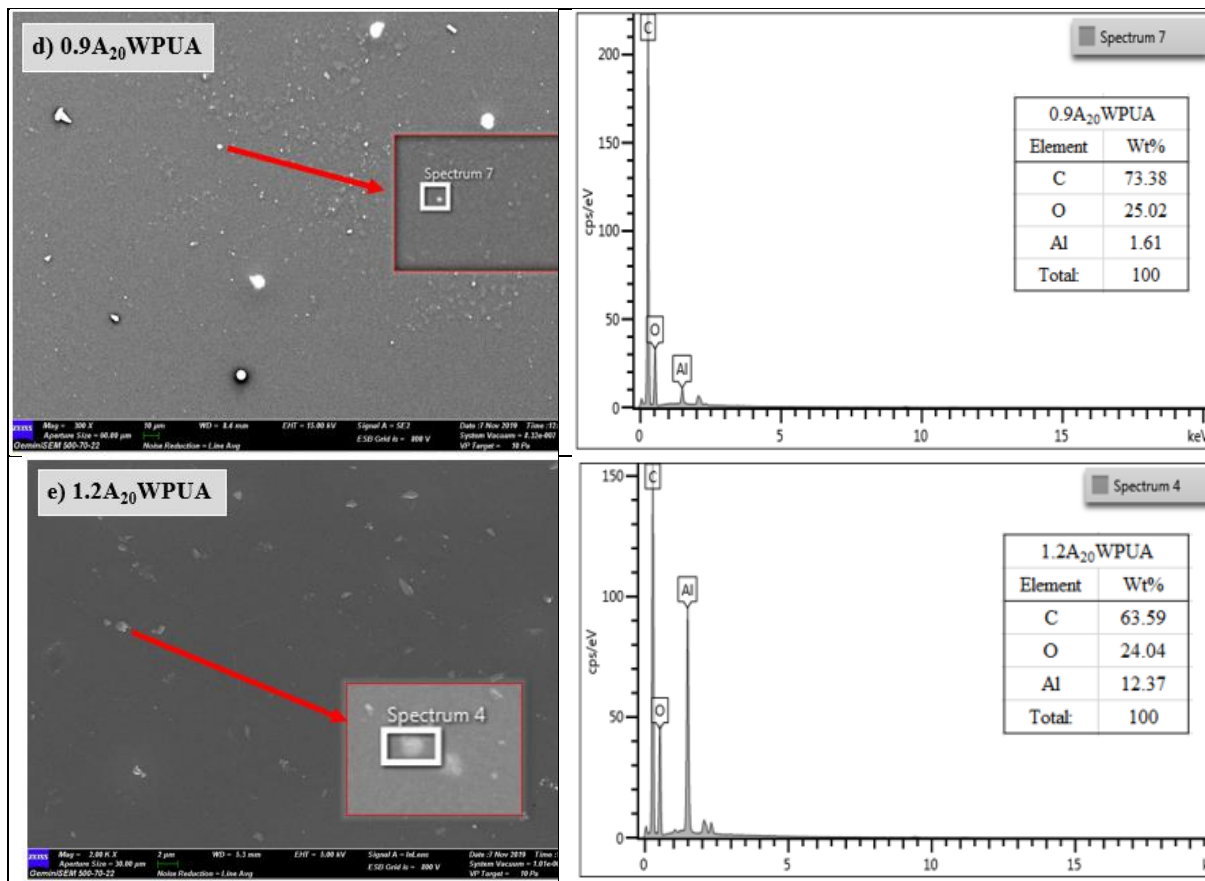


Figure 6. Morphology (FESEM) and energy dispersive X-ray analysis (EDX) spectrum of film coating, (a) Neat WPUA; (b) 0.3A₂₀WPUA; (c) 0.6A₂₀WPUA; (d) 0.9A₂₀WPUA; (e) 1.2A₂₀WPUA.

The purity and elemental composition of the WPUA/Al₂O₃ coatings were confirmed by the EDX measurement, as shown in Figure 6. EDX analysis confirms that only carbon (C), oxygen (O), and aluminum (Al) elements are present in the sample coatings, which is in good agreement with the stoichiometric composition of UV- WPUA/Al₂O₃ coatings. O, C, and Al are the main elements of WPUA/Al₂O₃ coatings, and the carbon peak belongs to both samples, which are neat WPUA and WPUA/Al₂O₃ coatings. The presence of Al and O element peak clearly showed the purity of Al₂O₃ nanoparticles (Figure 6 (b) - Figure 6(e)), and it confirmed the successful presence of Al₂O₃ in the samples. Atomic and weight percentages of the relevant elements are attached as an insert in their respective EDX graphs.

3.4. Coating characterization.

3.4.1. Glossiness.

The gloss values of surface coatings indicate that the UV-WPUA/Al₂O₃ coatings give a very high gloss surface. The values exceed 90 GU and 100 GU for measuring geometry of 60 ° and 20° for all tested coatings. Figure 7 shows the glossiness of UV-WPUA coatings with different compositions Al₂O₃ nanoparticles. The average gloss of neat WUA coatings was 148 GU. Incorporation of Al₂O₃ nanoparticles content up to 0.6 wt.% does not affect the glossiness of the coatings, while further increasing the nanoparticles up to 1.2 wt.% reduced the glossiness to 130 GU. The reason is that lower amounts of Al₂O₃ nanoparticles allow the coatings to flow more smoothly and uniformly. Another factor contributing to the high glossiness value is the smaller nanoparticles, and narrow size distribution particles fill the surface irregularities, providing a smoother surface with more compact air boundary surfaces [88,89].

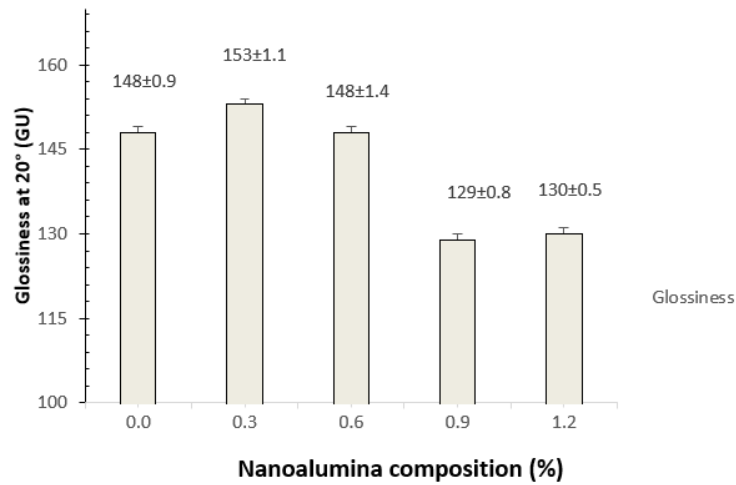


Figure 7. Glossiness of UV-WPUA/Al₂O₃ coating with different compositions Al₂O₃.

3.4.2. Water contact angle.

The static water contact angle was carried out to analyze the wettability or hydrophilic–hydrophobic properties of WPUA/Al₂O₃ coatings. Regarding water contact angles, it is accepted that a surface is hydrophilic if the contact angle value is less than 90° [90]. As illustrated in Figure 8, it was observed that the contact angles of neat WPUA coating is about 77.7° while a constant of 68.1° for WPUA/Al₂O₃ at different compositions between 0.3 – 0.9 wt%, showing hydrophilic properties, whereas the contact angles of WPUA/Al₂O₃ coatings decrease gradually to about 67.9° (12.4%) as the content of Al₂O₃ nanoparticles increased. However, the composition (0.3wt% - 1.2% wt) of Al₂O₃ nanoparticles embedded into WPUA dispersion was seen. The wettability value remains stable, which gives information that the composition of Al₂O₃ nanoparticles embedded into WPUA did not affect the wettability properties in the substrate tested. These results indicated that the wettability of the coating could be improved after the incorporation of Al₂O₃ nanoparticles, and this variation can be credited to the presence of an abundant surface hydroxyl group of Al₂O₃ nanoparticles. Furthermore, Al₂O₃ contributes to hydrophilicity due to particles themselves being hydrophilic (γ -Al₂O₃).

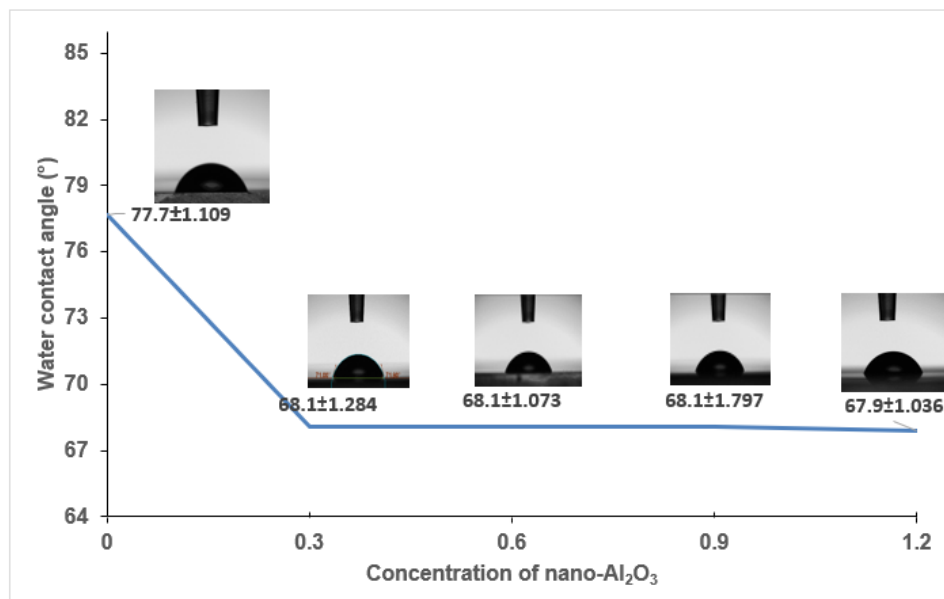


Figure 8. Static contact angle results of UV- WPUA/Al₂O₃ coating with different compositions Al₂O₃.

3.4.3. Pendulum hardness.

Hardness is the resistance of a material to localized plastic deformation [91]. Figure 9 shows the pendulum hardness of WPUA/nano- Al_2O_3 coatings as a function of nanoparticle content. It was found that the neat WPUA coatings show a pendulum hardness of 27.9 sec. The addition of 0.3, 0.6, 0.9 and 1.2 wt% of Al_2O_3 nanoparticles leads to mark pendulum hardness improvement around 63.4%, 63.4%, 28.8% and 4.7% respectively.

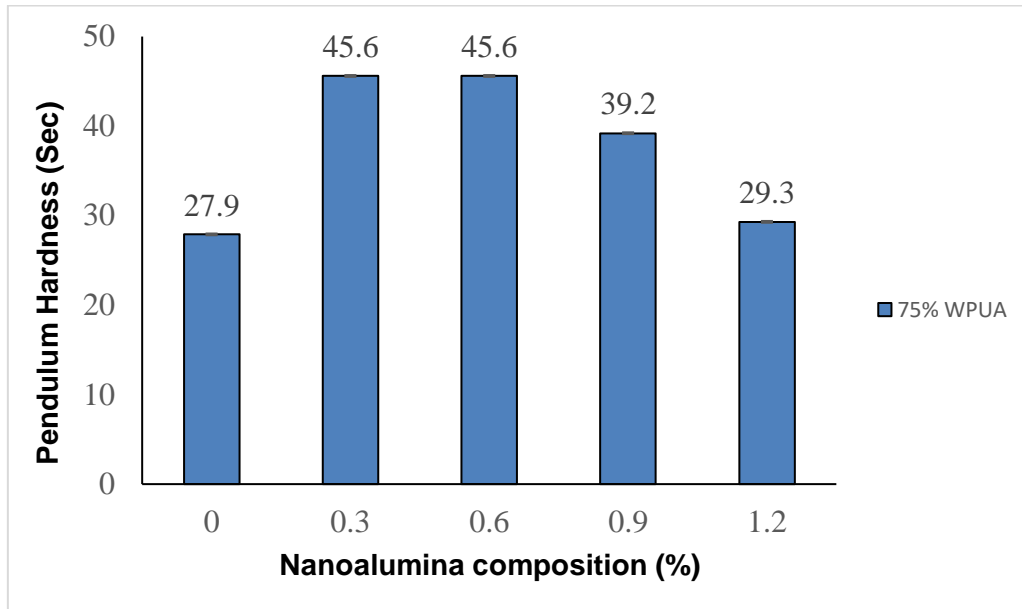


Figure 9. Pendulum hardness of UV-WPUA/ Al_2O_3 coating with different compositions of Al_2O_3 .

With an increase in the nano- Al_2O_3 content (0.3 to 1.2 wt%), the hardness of WPUA/nano- Al_2O_3 coatings increases and declines, but the hardness values are still high compared with unfilled ones nano- Al_2O_3 coatings. The hardness of WPUA coatings filled with 0.3 wt% and 0.6 wt% nano- Al_2O_3 content were the greatest values hardness among other compositions, which increased by 63.44% higher than that of 0 wt% nano- Al_2O_3 . The reason may be that adding a small amount of Al_2O_3 nanoparticles to the WPUA matrix could fill the pores arising from the water evaporation during the curable of WPUA and the contact areas between the WPUA matrix.

Since 0.3 wt.% and 0.6 wt.% nano- Al_2O_3 filled WPUA composite coated on glass substrates shows the highest value of hardness and hence selected as the optimal nano- Al_2O_3 content in WPUA. The addition of a small and optimal amount of nano- Al_2O_3 can exhibit strengthened and strong filler-matrix interaction, which plays an important role in improving the tribology properties of composites coating. Adding 0.9 wt.% and 1.2 wt.% nano- Al_2O_3 into the coating matrix can make their structure harder. Nevertheless, it is possibly also decreasing the hardness of the coating due to the increased roughness of the coating surface. Both contradictory impacts might challenge each other, pointing to a tiny variation in the hardness of the coating [92].

3.4.4. Pencil hardness and Scratch resistance.

The pencil hardness test is a standard industrial method that can roughly evaluate the short-term scratch resistance of the nanocomposite coatings [78,91,93,94]. Table 6 shows the result of pencil hardness and scratch resistance WPUA/ Al_2O_3 coatings. The pencil hardness

reveals continuous improvement with the increasing Al₂O₃ nanoparticles composition. As compared to the neat WPUA, it was noted that the increasing of Al₂O₃ nanoparticles raised the hardness of the coatings from H to a maximum of 5H. It has the most improvement in four higher grades up to 1.2 wt% nano-Al₂O₃ compositions. The improvement of pencil hardness owing to the addition of nanofillers has been reported by other researchers [78].

Table 6. Statistical data of pencil hardness and scratch-resistant of UV-WPUA/Al₂O₃ coatings using a diamond tip with 90°.

Sample code	Alumina Content (%)	Pencil hardness	Resistant to scratch, N
Neat PUA	0	2H±0.0	-
0.3A ₂₀ PU	0.3	4H±0.0	1.5±0.0
0.6A ₂₀ PU	0.6	4H±0.0	1.5±0.0
0.9A ₂₀ PU	0.9	5H±0.0	2.0±0.0
1.2A ₂₀ PU	1.2	5H±0.0	2.0±0.0

The incorporation of Al₂O₃ nanoparticles into the WPUA dispersion matrix improved the scratch resistance in all the cases tested compared to neat UV-WPUA coating. According to the results in Table 5, it was observed that neat UV-WPUA coatings failed at 0 N load, whereas the UV-WPUA/Al₂O₃ coatings could resist up to the 2 N load. This shows that the UV-WPUA/Al₂O₃ coatings have better scratch resistance compared to the neat UV-WPUA coatings. The improved scratch resistance of coatings after adding inorganic nanoparticles is mainly ascribed to the improved basic mechanical properties of nanocomposite coatings. After the scratch test, the scratched tracks of coatings were studied by an optical microscope. It can be found that the neat UV-WPUA coating fractured as early as the first round of the testing ended. The authors [95] reported that the pencil hardness of coatings reaches 4H-5H, enabling potential application as a protective film on PC covers for mobile phones.

3.4.5. Adhesion.

Based on the statistical analysis, the type of substrate significantly influenced the overall adhesion strength of the samples, while the type and layer thickness of coatings, as well as the number of layers applied to the surface of specimens, have not significantly affected the adhesion resistance of the panels used in this work. According to Table 7, the results show that all UV-WPUA/Al₂O₃ coatings (0.3 wt%, 0.6 wt%, 0.9 wt%, and 1.2 wt%) and neat WPUA coatings showed adhesion of 5B and 4B, respectively. These results refer to the ASTM standard (Table 4) for the cross-hatch adhesion test performed. It was observed that the WPUA/Al₂O₃ coatings had experienced no peeling with neat WPUA has experienced less than 5%. These results demonstrate that the Al₂O₃ nanoparticles are well dispersed in polymer matrices and enhance the adhesion strength of coatings performance. The authors [3] reported that poor dispersion of nanofillers in a polymer coating matrix could lead to low adhesion strength because close packing of nanoparticles often hides the hydroxyl groups required to form polar-polar bonds with the steel surface.

Table 7. Crosshatch adhesion of UV-WPUA/Al₂O₃ coatings.

Panel type	Sample designation	Alumina content (%)	Wet coating thickness (µm)	Average Adhesion strength
	Neat WPUA	0.0	120	4B
	0.3A ₂₀ WPUA	0.3	120	5B
Glass	0.6A ₂₀ WPUA	0.6	120	5B
	0.9A ₂₀ WPUA	0.9	120	5B
	1.2A ₂₀ WPUA	1.2	120	5B

4. Conclusions

The study aimed to develop UV-WPUA/Al₂O₃ coating properties superior to the neat coating. Renewable resource-based UV-WPUA/Al₂O₃ coatings were successfully prepared from jatropha oil, a renewable and sustainable resource, via *in situ* and anionic self-emulsifying methods. These coatings were cured by UV light. FTIR spectra indicated that EJO, JOL, and WPUA dispersion derived from jatropha oils successfully synthesized, and FESEM/EDX examinations of UV-WPUA/Al₂O₃ showed Al₂O₃ at the low concentration were well dispersed in the matrix. The incorporation of Al₂O₃ nanoparticles into WPUA dispersion demonstrates their ability to improve optical, mechanical simultaneously, and coating performances at low filler contents (0.3 – 1.2 wt.%). It was observed that the neat UV-WPUA coating is highly glossy and hydrophilic, with a water contact angle of 77.7°. The incorporation of Al₂O₃ nanoparticles in the coating has decreased the water contact angle to 12.36%. However, the water contact angle UV-WPUA/Al₂O₃ coatings remained almost constant compared to neat UV-WPUA coating. The pendulum hardness was greater than those of the neat WPUA coating, which was increased by 63.4% at filled 0.3 wt% Al₂O₃ nanoparticles. At a relatively low percentage loading Al₂O₃ nanoparticles content, UV-WPUA/Al₂O₃ coatings show excellent adhesion and good resistances toward scratch properties, including pencil hardness, compared to neat UV-WPUA. It is concluded from this work that the resulting UV-WPUA/Al₂O₃ nanoparticles transparent films are possibly interesting for the generation of UV-WPUA nanocomposite coatings with improved physical and mechanical properties provided by inorganic alumina nanoparticles.

Funding

This research was funded by the Ministry of Higher Education, Malaysia (MOHE) under Fundamental Research Grant Scheme (FRGS), with reference FRGS/1/2019/TK05/UPM/01/1 and Matching Grant Putra, UTM-UPM.

Acknowledgments

The authors gratefully acknowledge the Ministry of Higher Educations Malaysia and Universiti Kuala Lumpur for the financial support provided for this work. The authors would also like to thank the Malaysian Nuclear Agency and INTROP, Universiti Putra Malaysia, for technical support, and the use of their facilities and instruments. Many thanks also to Prof. Mohd. Azizan Mohd Noor for his comments.

Conflicts of Interest

The authors declare no conflict of interest.

References

1. Kim, M.S.; Ryu, K.M.; Lee, S.H.; Choi, Y.C.; Rho, S.; Jeong, Y.G. Chitin Nanofiber-Reinforced Waterborne Polyurethane Nanocomposite Films with Enhanced Thermal and Mechanical Performance. *Carbohydrate Polymers* **2021**, *258*, 117728, <http://doi.org/10.1016/j.carbpol.2021.117728>.
2. Zhu, Z.; Li, R.; Zhang, C.; Gong, S. Preparation and Properties of High Solid Content and Low Viscosity Waterborne Polyurethane—Acrylate Emulsion with a Reactive Emulsifier. *Polymers* **2018**, *10*, 154, <https://doi.org/10.3390/polym10020154>.

3. Skosana, S.J.; Khoathane, C.; Malwela, T. Enhancing the adhesion strength of polyurethane coatings by dispersing layered silicates via sonication and high-shear mixing method. *Polymer Bulletin* **2020**, <https://doi.org/10.1007/s00289-020-03100-y>.
4. Liu, X.; Hong, W.; Chen, X. Continuous Production of Waterborne Polyurethanes: A Review. *Polymers* **2020**, *12*, 2875, <https://doi.org/10.3390/polym12122875>.
5. Saalah, S.; Abdullah, L.C.; Aung, M.M.; Salleh, M.Z.; Awang Biak, D.R.; Basri, M.; Jusoh, E.R.; Mamat, S. Physicochemical Properties of Jatropha Oil-Based Polyol Produced by a Two Steps Method. *Molecules* **2017**, *22*, 551, <https://doi.org/10.3390/molecules22040551>.
6. Noble, K.L. Waterborne polyurethanes. *Prog. Org. Coat.* **1997**, *32*, 131–136, [https://doi.org/10.1016/s0300-9440\(97\)00071-4](https://doi.org/10.1016/s0300-9440(97)00071-4).
7. Banerjee, P.; Franco, A.; Chandra Babu Naidu K.; Suresh Kumar N. Water-borne Polyurethane-Metal Oxide Nanocomposite Applications. In: Inamuddin, Boddula R., Khan A. (eds) Sustainable Production and Applications of Waterborne Polyurethanes. Advances in Science, Technology & Innovation (IEREK Interdisciplinary Series for Sustainable Development). Springer, Cham. **2021**, https://doi.org/10.1007/978-3-030-72869-4_10.
8. Han, Y.; Hu, J.; Xin, Z. In-Situ Incorporation of Alkyl-Grafted Silica into Waterborne Polyurethane with High Solid Content for Enhanced Physical Properties of Coatings. *Polymers* **2018**, *10*, 514, <https://doi.org/10.3390/polym10050514>.
9. Kang, S.Y.; Ji, Z.; Tseng, L.F.; Turner, S.A.; Villanueva, D.A.; Johnson R.; Albano A.; Langer R. Design and Synthesis of Waterborne Polyurethanes. *Advanced Materials* **2018**, 1706237, <https://doi.org/10.1002/adma.201706237>.
10. Zafar, F.; Ghosal, A.; Sharmin, E.; Chaturvedi, R.; Nishat, N. A review on cleaner production of polymeric and nanocomposite coatings based on waterborne polyurethane dispersions from seed oils. *Progress in Organic Coatings* **2019**, *131*, 259–275, <https://doi.org/10.1016/j.porgcoat.2019.02.014>.
11. Noreen, A.; Zia, K.M.; Zuber, M.; Tabasum, S.; Saif, M.J. Recent trends in environmentally friendly waterborne polyurethane coatings: A review. *Korean Journal of Chemical Engineering* **2016**, *33*, 388–400.
12. Coogan, R.G. Post-crosslinking of waterborne urethanes. *Progress in Organic Coatings* **1997**, *32*, 51–63, [https://doi.org/10.1016/s0300-9440\(97\)00010-6](https://doi.org/10.1016/s0300-9440(97)00010-6).
13. Han, Y.; Jiang, Y.; Hu, J. Collagen incorporation into waterborne polyurethane improves breathability, mechanical property, and self-healing ability. *Composites Part A: Applied Science and Manufacturing* **2020**, 105854, <https://doi.org/10.1016/j.compositesa.2020.105854>.
14. Tremblay-Parrado, K.-K.; García-Astrain, C.; Avérous, L. Click chemistry for the synthesis of biobased polymers and networks derived from vegetable oils. *Green Chemistry* **2021**, *23*, 4296–4327, <http://doi:10.1039/d1gc00445j>.
15. Zhou, X.; Zhang, X.; Mengyuan, P.; He, X.; Zhang, C. Bio-based polyurethane aqueous dispersions. *Physical Sciences Reviews* **2021**, 20200075, <https://doi.org/10.1515/psr-2020-0075>.
16. Amri, M.R.; Al-Edrus, S.S.O.; Guan, C.T.; Md Yasin, F.; Hua, L.S. Jatropha Oil as a Substituent for Palm Oil in Biobased Polyurethane. *International Journal of Polymer Science* **2021**, *2021*, 6655936, <https://doi.org/10.1155/2021/6655936>.
17. Aung, M.M.; Yaakob, Z.; Kamarudin, S.; Abdullah, L.C. Synthesis and characterization of Jatropha (*Jatropha curcas* L.) oil-based polyurethane wood adhesive. *Industrial Crops and Products* **2014**, *60*, 177–185, <https://doi.org/10.1016/j.indcrop.2014.05.038>.
18. Patil, C.K.; Jung, D.W.; Jirimali, H.D.; Baik, J.H.; Gite, V.V.; Hong, S.C. Nonedible Vegetable Oil-Based Polyols in Anticorrosive and Antimicrobial Polyurethane Coatings. *Polymers* **2021**, *13*, 3149, <https://doi.org/10.3390/polym13183149>.
19. Amri, M.R.; Md Yasin, F.; Abdullah, L.C.; Al-Edrus, S.S.O.; Mohamad, S.F. Ternary Nanocomposite System Composing of Graphene Nanoplatelet, Cellulose Nanofiber and Jatropha Oil Based Waterborne Polyurethane: Characterizations, Mechanical, Thermal Properties and Conductivity. *Polymers* **2021**, *13*, 3740, <https://doi.org/10.3390/polym13213740>.
20. Amri, M.R.; Guan, C.T.; Osman Al-Edrus, S.S.; Md Yasin, F.; Mohamad, S.F. Effect of Cellulose Nanofibrils on the Properties of Jatropha Oil-Based Waterborne Polyurethane Nanocomposite Film. *Polymers* **2021**, *13*, 1460, <https://doi.org/10.3390/polym13091460>.
21. Saalah S.; Abdullah L.C.; Aung M.M.; Salleh M.Z.; Awang Biak D.R.; Basri M.; Jusoh E.R.; Mamat S. Colloidal stability and rheology of jatropha oil-based waterborne polyurethane (JPU) dispersion. *Prog. Org. Coat.* **2018**, *125*, 348–357, <https://doi.org/10.1016/j.porgcoat.2018.09.018>.

22. Saalah, S.; Abdullah, L.C.; Aung, M.M.; Salleh, M.Z.; Awang Biak, D.R.; Basri, M.; Jusoh, E.R.; Mamat, S.; Osman, Al Edrus, S.S. Chemical and Thermo-Mechanical Properties of Waterborne Polyurethane Dispersion Derived from Jatropha Oil. *Polymers* **2021**, *13*, 795, <https://doi.org/10.3390/polym13050795>.
23. Saravari, O.; Praditvatanakit S. Preparation and properties of urethane alkyd based on a castor oil/jatropha oil mixture. *Prog. Org. Coat.* **2013**, *76*, 698–704, <https://doi.org/10.1016/j.porgcoat.2012.12.012>.
24. Harjono; Sugita, P.; Mas'ud, Z.A. Synthesis and application of jatropha oil-based polyurethane as paint coating material. *Makara. J. Sci.* **2012**, *16*, 134–140, <https://doi.org/10.7454/mss.v16i2.1409>.
25. Tuan Naiwi, T.S.R.; Aung, M.; Ahmad, A.; Rayung, M.; Su'ait, M.; Yusof, N.; Wynn, L.K. Enhancement of Plasticizing Effect on Bio-Based Polyurethane Acrylate Solid Polymer Electrolyte and Its Properties. *Polymers* **2018**, *10*, 1142, <https://doi.org/10.3390/polym10101142>.
26. Chai, K.L.; Aung, M.M.; Rayung, M.; Abdullah, L.C.; Lim, H.N.; Mohd Noor, I.S. Performance of Ionic Transport Properties in Vegetable Oil-Based Polyurethane Acrylate Gel Polymer Electrolyte. *ACS Omega* **2019**, *4*, 2554–2564, <https://doi.org/10.1021/acsomega.8b02100>.
27. Rayung, M.; Aung, M.M.; Su'ait, M.S.; Abdullah, L.C.; Ahmad, A.; Lim, H.N. Performance Analysis of Jatropha Oil-Based Polyurethane Acrylate Gel Polymer Electrolyte for Dye-Sensitized Solar Cells. *ACS Omega* **2020**, *acsomega9b*, 4348, <https://doi.org/10.1021/acsomega.9b04348>.
28. Dong, F.; Maganty, S.; Meschter, S.J.; Cho, J.H. Effects of curing conditions on structural evolution and mechanical properties of UV-curable polyurethane acrylate coatings. *Prog. Org. Coat.* **2018**, *114*, 58–67, <https://doi.org/10.4028/www.scientific.net/AMR.197-198.1281>.
29. Li, J.; Yin, Y.; Yaseen, M.; Yang, J.; Yang, S.; Yang, H.; Sahibzada, M. Preparation and Properties of Modified Graphene Oxide Incorporated Waterborne Polyurethane Acrylate. *Polymer International* **2019**, <https://doi.org/10.1002/pi.5799>.
30. Zhu, Z.; Li, R.; Zhang, C.; Gong, S. Preparation and Properties of High Solid Content and Low Viscosity Waterborne Polyurethane—Acrylate Emulsion with a Reactive Emulsifier. *Polymers* **2018**, *10*, 154, <https://doi.org/10.3390/polym10020154>.
31. Zhang, D.; Liu, J.; Li, Z.; Shen, Y.; Wang, P.; Wang, D.; Hu, X. Preparation and properties of UV-curable waterborne silicon-containing polyurethane acrylate emulsion. *Progress in Organic Coatings* **2021**, *160*, <https://doi.org/10.1016/j.porgcoat.2021.106503>.
32. Xu, J.C.; Rong, X.S.; Chi, T.Y.; Wang, M.; Wang, Y.Y.; Yang, D.Y.; Qiu, F.X. Preparation, characterization of UV-curable waterborne polyurethane-acrylate and the application in metal iron surface protection. *Journal of Applied Polymer Science* **2013**, *130*, 3142–3152, <https://doi.org/10.1002/app.39539>.
33. Xu, J.; Jiang, Y.; Qiu, F.; Dai, Y.; Yang, D.; Yu, Z.; Yang, P. Synthesis, mechanical properties and iron surface conservation behavior of UV-curable waterborne polyurethane-acrylate coating modified with inorganic carbonate. *Polymer Bulletin* **2018**, <https://doi.org/10.1007/s00289-018-2294-1>.
34. Nayini, M.M.R.; Bastani, S.; Moradian, S.; Crout'e-Barghorn, C.; Allonas, X. Manipulating the surface structure of hybrid UV curable coatings through photopolymerization-induced phase separation: influence of inorganic portion and photoinitiator content. *Macromolecular Chemistry and Physics* **2018**, 1700377, <https://doi.org/10.1002/macp.201700377>.
35. Li, C.; Xiao, H.; Wang, X.; Zhao, T. Development of green waterborne UV-curable vegetable oil-based urethane acrylate pigment prints adhesive: Preparation and application. *Journal of Cleaner Production* **2018**, *180*, 272–279, <https://doi.org/10.1016/j.jclepro.2018.01.193>.
36. Liu, C.; Wang, C.; Hu, Y.; Zhang, F.; Shang, Q.; Lei, W.; Zhou, Y.; Cai, Z. Castor oil-based polyfunctional acrylate monomers: Synthesis and utilization in UV-curable materials. *Progress in Organic Coatings* **2018**, *121*, 236–246, <https://doi.org/10.1016/j.porgcoat.2018.04.020>.
37. Moon, J.H.; Shul, Y.G.; Hong, S.Y.; Choi, Y.S.; Kim, H.T. A study on UV-curable adhesives for optical pick-up: I. Photo-initiator effects. *International Journal of Adhesion and Adhesives* **2005**, *25*, 301–312.
38. Fu, J.; Wang, L.; Yu, H.; Haroon, M.; Haq, F.; Shi, W.; Wu, B.; Wang, L. Research progress of UV-curable polyurethane acrylate-based hardening coatings. *Progress in Organic Coatings* **2019**, *131*, 82–99, <https://doi.org/10.1016/j.porgcoat.2019.01.061>.
39. Wang, X.; Zhan, J.; Xing, W.; Wang, X.; Song, L.; Qian, X.; Yu, B.; Hu, Y. Flame retardancy and thermal properties of novel UV-curable epoxy acrylate coatings modified by a silicon-bearing hyperbranched polyphosphonate acrylate, *Ind. Eng. Chem. Res.* **2013**, *52*, 5548–5555.
40. Qin, L.; He, Y.; Liu, B.; Jian, Y.; Li, C.; Nie, J. Preparation and properties of polyurethane acrylates modified by saturated alcohols, *Progress in Organic Coating* **2013**, *76*, 1594–1599.

41. Liu, R.; Zheng, J.; Guo, R.; Luo, J.; Yuan, Y.; Liu, X. Synthesis of new biobased antibacterial methacrylates derived from tannic acid and their application in UV-cured coatings, *Ind. Eng. Chem. Res.* **2014**, *53*, 10835–10840.
42. Najafi, F.; Bakhshandeh, E.; Hadavand, B.S.; Saeb, M.R. Toward UV-curable urethane acrylate/silica hybrid coatings: Introducing urethane methacrylate trimethoxysilane (UAMS) as organic-inorganic coupling agent, *Prog. Org. Coat.* **2014**, *77*, 1957–1965.
43. Flores, M.; Fernandez-Francos, X.; Ramis, X.; Sangermano, M.; Ferrando, F.; Serra, A. Photocuring of cycloaliphatic epoxy formulations using polyesters with multiarm star topology as additives. *J. Appl. Polym. Sci.* **2014**, *131*, 596–602.
44. Dai, J.; Liu, X.; Ma, S.; Wang, J.; Shen, X.; You, S.; Zhu, J. Soybean oil-based UVcurable coatings strengthened by crosslink agent derived from itaconic acid together with 2-hydroxyethyl methacrylate phosphate. *Prog. Org. Coat.* **2016**, *97*, 210–215.
45. Choi, S.; Lee, M.; Shin, E. One-Pot Processing of Regenerated Cellulose Nanoparticles/Waterborne Polyurethane Nanocomposite for Eco-friendly Polyurethane Matrix. *Polymers* **2019**, *11*, 356, <https://doi.org/10.3390/polym11020356>.
46. Saalah, S.; Abdullah L.C.; Aung M.M; Salleh M.Z.; Awang Biak D.R.; Basri M.; Jusoh E.R. Waterborne polyurethane dispersions synthesized from jatropha oil. *Industrial Crops and Products* **2015**, *64*, 194–200, <https://doi.org/10.1016/j.indcrop.2014.10.046>.
47. Liu, J.; Cao, J.; Zhou, Z.; Liu, R.; Yuan, Y.; Liu, X. Stiff Self-Healing Coating Based on UV-Curable Polyurethane with a "Hard Core, Flexible Arm" Structure. *ACS Omega* **2018**, *3*, 11128–11135, <https://doi.org/10.1021/acsomega.8b00925>.
48. Abdeen, D.; El Hachach, M.; Koc, M.; Atieh, M.A Review on the Corrosion Behaviour of Nanocoatings on Metallic Substrates. *Materials* **2019**, *12*, 210, <https://doi.org/10.3390/ma12020210>.
49. Islam, Md.M.; Shakil, S.I.; Shaheen, N.M.; Bayati, P.; Haghshenas, M. An overview of microscale indentation fatigue: Composites, thin films, coatings, and ceramics. *Micron* **2021**, *148*, 103110, <https://doi.org/10.1016/j.micron.2021.103110>.
50. Ren, H.; Zhou, Y.; He, M.; Xu, R.; Ding, B.; Zhong, X.; Tong, Y.; Fan, L.; Cai, Z.; Shen, H.; Huang, Y. Enhanced mechanical properties of silica nanoparticle-covered cross-linking graphene oxide filled thermoplastic polyurethane composite. *New Journal of Chemistry* **2018**, *42*, 3069–3077, <https://doi.org/10.1039/C7NJ03503A>.
51. Maganty, S.; Roma, M P.C.; Meschter, S.J.; Starkey, D.; Gomez, M.; Edwards, D.G.; Ekin, A.; Elsken, K.; Cho, J. Enhanced mechanical properties of polyurethane composite coatings through nanosilica addition. *Progress in Organic Coatings* **2016**, *90*, 243–251, <https://doi.org/10.1016/j.porgcoat.2015.10.016>.
52. Bai, Y.; Zhang, H.; Shao, Y.; Zhang, H.; Zhu, J. Recent Progresses of Superhydrophobic Coatings in Different Application Fields: An Overview. *Coatings* **2021**, *11*, 116, <https://doi.org/10.3390/coatings11020116>.
53. Ching, Y.C.; Ching, Y.C.; Yaacob, I. Effect of polyurethane/nanosilica composite coating on thermomechanical properties of polyethylene film. *Materials Technology* **2012**, *27*, 113–115, <https://doi.org/10.1179/175355511X13240279340246>.
54. Malaki, M.; Hashemzadeh, Y.; Karevan, M. Effect of nano-silica on the mechanical properties of acrylic polyurethane coatings. *Progress in Organic Coatings* **2016**, *101*, 477–485, <https://doi.org/10.1016/j.porgcoat.2016.09.012>.
55. Ariffin, M.M; Aung, M.M; Abdullah, L.C; Salleh, M.Z. Assessment of corrosion protection and performance of bio-based polyurethane acrylate incorporated with nano zinc oxide coating. *Polymer Testing* **2020**, *87*, 106526, <http://doi.org/10.1016/j.polymertesting.2020.106526>.
56. Mastouri Mansourabad, A.; Azadfallah, M.; Tarmian, A.; Efhami, Sisi D. Nano-cerium dioxide synergistic potential on abrasion resistance and surface properties of polyurethane-nanocomposite coatings for esthetic and decorative applications on wood. *Journal of Coatings Technology and Research* **2020**, <https://doi.org/10.1007/s11998-020-00374-9>.
57. Swain, S.; Sharma, R.A.; Bhattacharya, S.; Chaudhary, L. Effects of Nano-silica/Nano-alumina on Mechanical and Physical Properties of Polyurethane Composites and Coatings. *Trans. Electr. Electron. Mater* **2013**, *14*, 1–8.
58. Lazouzi, G.; Vuksanović, M.M.; Tomić, N.Z.; Mitrić, M.; Petrović, M.; Radojević, V.; Hainemann, R.J. Optimized preparation of alumina based fillers for tuning composite properties. *Ceramics International* **2018**, *S0272884218300944*, <https://doi.org/10.1016/j.ceramint.2018.01.083>.

59. Kajohnchaiyagual, J.; Jubsilp, C.; Dueramae, I.; Rimdusit, S. Thermal and mechanical properties enhancement obtained in highly filled alumina-polybenzoxazine composites. *Polymer Composites* **2014**, *35*, 2269–2279, <https://doi.org/10.1002/pc.22892>.
60. Pakseresht, A.H.; Saremi, M.; Omidvar, H.; Alizadeh, M. Micro-structural study and wear resistance of thermal barrier coating reinforced by alumina whisker. *Surface and Coatings Technology* **2019**, *366*, 338–348, <https://doi.org/10.1016/j.surfcoat.2019.03.059>.
61. Maurya, S.D.; Kurmvanshi, S.K.; Mohanty, S.; Nayak, S.K. A Review on Acrylate-Terminated Urethane Oligomers and Polymers: Synthesis and Applications. *Polym. Plast. Technol. Eng.* **2018**, *57*, 625–656.
62. Chen, H.; Li, C.; Yao, Q.; Chen, F.; Fu, Q. Enhanced thermal conductivity and wear resistance of polytetrafluoroethylene via incorporating hexagonal boron nitride and alumina particles. *Journal of Applied Polymer Science* **2021**, 51497, <https://doi.org/10.1002/app.51497>.
63. Wagih, A.; Fathy, A. Improving compressibility and thermal properties of Al–Al₂O₃ nanocomposites using Mg particles. *Journal of Materials Science* **2018**, *53*, 11393–11402, <https://doi.org/10.1007/s10853-018-2422-1>.
64. Abyzov, A.M. Aluminum Oxide and Alumina Ceramics (review). Part 1. Properties of Al₂O₃ and Commercial Production of Dispersed Al₂O₃. *Refractories and Industrial Ceramics* **2019**, <https://doi.org/10.1007/s11148-019-00304-2>.
65. Roy, S.K.; Moorthy, V.K. Alumina Special Ceramics. *Transactions of the Indian Ceramic Society* **1981**, *40*, 212–216, <https://doi.org/10.1080/0371750X.1981.10822552>.
66. Sung, L.P.; Comer, J.; Forster, A.M.; Hu, H.; Floryancic, B.; Brickweg, L.; Fernando, R.H. Scratch behavior of nano-alumina/polyurethane coatings. *J. Coat. Technol. Res.* **2008**, *5*, 419–430, <https://doi.org/10.1007/s11998-008-9110-z>.
67. Nguyen, T.P. Radically curable nano-based coatings. *Nanomaterials-based Coatings* **2019**, 339–372, <https://doi.org/10.1016/B978-0-12-815884-5.00010-7>.
68. George, J.; Ishida, H. A review on the very high nanofiller-content nanocomposites: Their preparation methods and properties with high aspect ratio fillers. *Progress in Polymer Science* **2018**, *86*, 1–39, <https://doi.org/10.1016/j.progpolymsci.2018.07.006>.
69. Liu, F.; Liu, A.; Tao, W.; Yang, Y. Preparation of UV curable organic/inorganic hybrid coatings-a review. *Progress in Organic Coatings* **2020**, *145*, 105685, <https://doi.org/10.1016/j.porgcoat.2020.105685>.
70. Ansoorge, S.; Papailiou, K. Mechanical properties of silicone rubber under high loadings of alumina trihydrate filler. *Journal of Elastomers and Plastics* **2015**, 0095244315580452, <https://doi.org/10.1177/0095244315580452>.
71. Mohammed, A. UHMWPE Nanocomposite Coatings Reinforced with Alumina (Al₂O₃) Nanoparticles for Tribological Applications. *Coatings* **2018**, *8*, 280, <https://doi.org/10.3390/coatings8080280>.
72. Arun, A.; Sathiyamoorthy, V.; Vivek Anand, S.M.K.; Ganesh Boopathy, V.; Prasanth, R. Tribological studies on properties of Al₂O₃ reinforced Ultra high molecular weight polyethylene. *J. Chem. Pharm. Sci.* **2017**, *2*, 186–189.
73. Saha, D.; Bose, P.K.; Banthia, A.K.; Dhabal, S. Analysis and Characterization of Alumina Particles Reinforced Ultra High Molecular Weight Polyethylene Composite for Acetabular Cup. *The International Journal of Artificial Organs* **2007**, *30*, 144–152, <https://doi.org/10.1177/039139880703000209>.
74. Ezzat, A.A.; Mousa, M.O.; Ali, W.Y. Influence of aluminum oxide nanofibers reinforcing polyethylene coating on the abrasive wear. *Friction and Wear Research* **2016**, *4*, 1–13, <https://doi.org/10.14355/fwr.2016.04.001>.
75. Chanda, A.; Mukhopadhyay, A.K.; Basu, D.; Chatterjee, S. Wear and friction behaviour of UHMWPE-alumina combination for total hip replacement. *Ceram. Int.* **1997**, *23*, 437–447, [https://doi.org/10.1016/s0272-8842\(96\)00052-1](https://doi.org/10.1016/s0272-8842(96)00052-1).
76. Roy, S.; Pal, S. Characterization of silane coated hollow sphere alumina-reinforced ultra-high molecular weight polyethylene composite as a possible bone substitute material. *Bull. Mater. Sci.* **2002**, *25*, 609–612, <https://doi.org/10.1007/bf02707893>.
77. ASTM D7027-05: Standard Test Method for Evaluation of Scratch Resistance of Polymeric Coatings and Plastics Using an Instrumented Scratch Machine; ASTM International: West Conshohocken, PA, USA, 2005; Available online: <https://www.astm.org/DATABASE.CART/HISTORICAL/D7027-05.htm> (accessed on 23 March **2018**).

78. Zhang, H.; Zhang, H.; Tang, L.; Zhang, Z.; Gu, L.; Xu, Y.; Eger, C. Wear-resistant and transparent acrylate-based coating with highly filled nanosilica particles. *Tribology International* **2010**, *43*, 83–91, <https://doi.org/10.1016/j.triboint.2009.05.022>.
79. Hazmi, A.S.A.; Aung, M.M.; Abdullah, L.C.; Salleh, M.Z.; Mahmood, M.H. Producing Jatropha oil-based polyol via epoxidation and ring opening. *Industrial Crops and Products* **2013**, *50*, 563–567, <https://doi.org/10.1016/j.indcrop.2013.08.003>.
80. Jusoh Taib, E.R.; Abdullah, L.C.; Aung, M.M.; Basri, M.; Salleh, M.Z.; Saalah, S.; Mamat, S.; Chee, C.Y.; Wong J.L.; Lin L. Physico-chemical characterisation of epoxy acrylate resin from jatropha seed oil. *Pigment & Resin Technology* **2017**, 00–00, <https://doi.org/10.1108/prt-11-2016-0116>.
81. Xiaoyang, M.; Zemin, Q.; Zhifeng, H.; Xinli, J. The dependence of pendulum hardness on the thickness of acrylic coating. *J. Coat. Technol. Res.* **2013**, *10*, 433–439, <https://doi.org/10.1007/s11998-013-9477-3>.
82. Petrovic, Z.S. Polyurethanes from Vegetable Oils. *Polymer Reviews.* **2008**, *48*, 109–155, <https://doi.org/10.1080/15583720701834224>.
83. Taung Mai, L.L.; Aung, M.M.; Muhamad Saidi, S.A.; San H'ng P.; Rayung, M.; Mohamad Jaafar, A. Non Edible Oil-Based Epoxy Resins from Jatropha Oil and Their Shape Memory Behaviors. *Polymers* **2021**, *13*, 2177, <https://doi.org/10.3390/polym13132177>.
84. Yin, Y.; Muhammad, Y.; Zeng, X.; Yang, J.; Li, J.; Yang, S.; Zhao, Z.; Subhan, S. Synthesis and properties of octadecylamine-graphene oxide modified highly hydrophobic waterborne polyurethane emulsion. *Progress in Organic Coatings* **2018**, *125*, 234–241, <https://doi.org/10.1016/j.porgcoat.2018.09.005>.
85. Dai, Y.T.; Qiu, F.X.; Xu, J.C.; Yu, Z.P.; Yang, P.F.; Xu, B.B.; Jiang, Y.; Yang, D.Y. Preparation and properties of UV-curable waterborne graphene oxide/polyurethane-acrylate composites. *Plastics, Rubber and Composites* **2014**, *43*, 54–62, <https://doi.org/10.1179/1743289813y.0000000071>.
86. Feng, J.; Ye, D. Polymerizable ZnO photoinitiators of surface modification with hydroxyl acrylates and photopolymerization with UV-curable waterborne polyurethane acrylates. *European Polymer Journal* **2019**, *120*, 109252–, <https://doi.org/10.1016/j.eurpolymj.2019.109252>.
87. Ma, P.C.; Siddiqui, N.A.; Marom, G.; Kim J.K. Dispersion and functionalization of carbon nanotubes for polymer-based nanocomposites: A review. *Composites: Part A* **2010**, *41*, 0–1367, <https://doi.org/10.1016/j.compositesa.2010.07.003>.
88. Ding, Z.; Li, J.; Xin, W.; Zhu, J.; Luo, Y. Matte waterborne polyurethane fabric nanocoating with versatility via mono-layered montmorillonite nanosheets. *Progress in Organic Coatings* **2021**, *159*, 106420, <https://doi.org/10.1016/j.porgcoat.2021.106420>.
89. Lee, D.I. A Fundamental Study on Coating Gloss. Presented at the 25th Annual TAPPI Coating Conference, May, 1974 and published in *TAPPI Coating Conference Proceeding, Atlanta GA* **1974**, 97–114.
90. Liu, Q.; Liao, B.; Pang, H.; Lu, M.; Meng, Y. Preparation and characterization of a self-matting coating based on waterborne polyurethane-polyacrylate hybrid dispersions. *Progress in Organic Coatings* **2020**, *143*, 105551, <https://doi.org/10.1016/j.porgcoat.2020.105551>.
91. Zhang, H.K.; Xiao, H.; Fang, X.W.; Zhang, Q.; Logé, R.E.; Huang, K. A critical assessment of experimental investigation of dynamic recrystallization of metallic materials. *Materials & Design* **2020**, *193*, 108873, <https://doi.org/10.1016/j.matdes.2020.108873>.
92. Nguyen, T.V.; Do, T.V.; Ha, M.H.; Le, H.K.; Le, T.T.; Linh Nguyen, T.N.; Dam, X.T.; Lu, L.T.; Tran, D.L.; Vu Quoc, T.; Dinh, D.A.; Dang, T.C.; Nguyen – Tri, P. Crosslinking process, mechanical and antibacterial properties of UV-curable acrylate/Fe₃O₄-Ag nanocomposite coating. *Progress in Organic Coatings* **2019**, 105325–, <https://doi.org/10.1016/j.porgcoat.2019.105325>.
93. Wang, X.; Xing, W.; Song, L.; Yu, B.; Hu, Y.; Yeoh, G.H. Preparation of UV-curable functionalized graphene/polyurethane acrylate nanocomposite with enhanced thermal and mechanical behaviors. *React. Funct. Polym.* **2013**, *73*, 854–858, <https://doi.org/10.1016/j.reactfunctpolym.2013.03.003>.
94. Lee, C.; Wei, X.; Kysar, J.W.; Hone, J. Measurement of the elastic properties and intrinsic strength of monolayer graphene. *Science* **2008**, *321*, 385–388, <https://doi.org/10.2307/20054532>.
95. Parsimehr, H.; Langroudi, A.E. Waterborne Polyurethane-Polyacrylate Hybrids. In: Inamuddin, Boddula R., Khan A. (eds) Sustainable Production and Applications of Waterborne Polyurethanes. Advances in Science, Technology & Innovation (IEREK Interdisciplinary Series for Sustainable Development). Springer, Cham. **2021**, https://doi.org/10.1007/978-3-030-72869-4_2.